NiO as a test case for high resolution resonant inelastic soft x-ray scattering

2005 J. Phys.: Condens. Matter 17 5397

(http://iopscience.iop.org/0953-8984/17/35/007)

INSTITUTE OF PHYSICS PUBLISHING JOURNAL OF PHYSICS: CONDENSED MATTER

J. Phys.: Condens. Matter **17** (2005) 5397–5412 doi:10.1088/0953-8984/17/35/007

NiO as a test case for high resolution resonant inelastic soft x-ray scattering

G Ghiringhelli[1], M Matsubara[2], C Dallera[1], F Fracassi[1], R Gusmeroli[3], A Piazzalunga[1], A Tagliaferri[1], N B Brookes[4], A Kotani[5,6] and L Braicovich[1]

[1] INFM—Dipartimento di Fisica, Politecnico di Milano, piazza Leonardo da Vinci 32, 20133 Milano, Italy
[2] Institute for Solid State Physics, University of Tokyo, 5-1-5, Kashiwanoha, Kashiwa, Chiba 277-8581, Japan
[3] Dipartimento di Elettronica e Informazione, Politecnico di Milano, piazza Leonardo da Vinci 32, 20133 Milano, Italy
[4] European Synchrotron Radiation Facility, BP 220, 38043 Grenoble Cédex, France
[5] RIKEN/SPring-8, 1-1-1, Mikazuki-cho, Sayo-gun, Hyogo 679-5148, Japan
[6] Photon Factory, Institute of Materials Structure Science, 1-1 Oho, Tsukuba, Ibaraki 305-0801, Japan

E-mail: giacomo.ghiringhelli@fisi.polimi.it

Received 30 May 2005, in final form 27 July 2005
Published 19 August 2005
Online at stacks.iop.org/JPhysCM/17/5397

Abstract

Resonant inelastic x-ray scattering (RIXS) at the $L_{2,3}$ edges of 3d transition metal compounds has recently become a high resolution spectroscopic technique thanks to improvements in the instrumentation. We have chosen the prototypical case of NiO to explore the various levels of interpretation applicable to L_3 RIXS spectra of strongly correlated electron systems. Starting from a set of experimental data measured across the Ni L_3 absorption edge with 550 meV combined energy resolution, we analyse the rich spectral structure within an atomic framework. The spectra can be separated into dd and charge transfer excitation regions. The dd excitations can be interpreted and well reproduced within a crystal field model. The charge transfer excitations are analysed through the comparison with calculations made in the Anderson impurity model. A series of parameters belonging to the proposed models (crystal field strength, charge transfer energy, hybridization integrals) can thus be extracted in a very direct and unambiguous way.

(Some figures in this article are in colour only in the electronic version)

1. Introduction

The search for a correct description of the electronic and magnetic structure of solids is often based on a variety of spectroscopic measurements that bring information on the excited states

rather than on the ground state of the system under analysis. The main qualities of any spectroscopic technique are the sensitivity to the relevant properties and the simplicity of the interpretation framework. Both are strong points of photoemission and optical spectroscopies like optical absorption or Raman scattering. Conversely, in resonant x-ray spectroscopies the excellent sensitivity and selectivity are counterbalanced by the difficult interpretation of the experimental spectra. The information content can be deciphered only through sophisticated simulations, which have to account both for the electronic structure of the sample and for the exact spectroscopic processes in use. We present here evidence that resonant inelastic x-ray scattering (RIXS) is now becoming a noticeable exception among the resonant spectroscopies, at least in the cases of samples exhibiting a strongly correlated electronic structure. RIXS spectra as performed with soft x-rays can be relatively simple to interpret and they keep the sensitivity and selectivity typical of x-ray absorption spectroscopy. In fact, similar to optical spectroscopy, RIXS provides a mapping of the neutral electronic excitations in the sample: dd and ff excitations, charge transfer excitations, spin-flip and exchange excitations. Moreover it is not limited by electric dipole selection rules of direct transitions and the resonance selects the chemical species and, in some cases, the crystalline site. Electron beams are not involved in the detection or excitation, so with soft x-ray RIXS the sample is probed in depth and insulating materials can be studied as well as conductors. We recall that in photoemission the surface state contribution becomes negligible only when using hard x-rays, and electrostatic charging can always be a major problem.

In RIXS a photon is resonantly absorbed and re-emitted in a second order process that leaves the system in an excited state. The energy difference between the incident and re-emitted photons gives the energy of the resulting excitation. The polarization of the radiation, the sample crystalline and magnetization orientation, and the scattering geometry are parameters that influence the intensity of the measured excitations, as opposed to their energy (if we neglect the photon momentum transferred to the sample). Usually the relevant excitations lie between zero and a few electronvolts. The excitation photon energy can be tuned at the absorption edges of the various chemical elements in the sample, and different excitation edges can be investigated. The choice of the excitation step can be influenced both by issues related to the sample (strong resonant enhancement, transition to valence states more or less hybridized with neighbouring atoms) or involving the scattering process itself (cross section, available source, instrumental energy resolution).

In the present paper we explore NiO as a paradigmatic member of the vast and fascinating family of 3d transition metal oxides. In NiO RIXS can be performed at the K, $L_{2,3}$ or $M_{2,3}$ edges of Ni, or at the K edge of oxygen. We concentrate here on the L_3 edge RIXS: the excitation and de-excitation are made through transitions to and from the 3d electrons of Ni, whose dominant local character is accompanied by a non-negligible hybridization with the 2p states of oxygen. In principle L and M edge RIXS are thus equally suited for the study of the 3d states and their neutral excitations, although some practical and fundamental differences have to be considered and will be discussed briefly below. On the other hand Ni and O K edge RIXS (one in the hard x-rays and the other in the soft x-ray range) are better indicated in the study of delocalized states: noticeable examples were published in the recent years on manganites and cuprates, where the interplay of 3d correlation and band formation is crucial [1–4]. In this paper we focus on the local excitations of NiO (dd excitations, charge transfer excitations, and inter-atomic exchange excitations), trying to extract the maximum of information from L_3 edge RIXS spectra.

The great potential of RIXS has been little exploited until now mainly due to experimental difficulties. The measurements require a monochromator for the incident beam and a spectrometer for the scattered radiation: the two instruments equally contribute to the final

energy resolution. The $L_{2,3}$ edges of 3d transition metals are very advantageous for the strong resonant enhancement and for the sensitivity of the absorption (excitation) process to the chemical and magnetic properties of the sample. On the other hand these edges fall in the soft x-ray range (400–1000 eV) where grazing incidence gratings are needed both for monochromators and spectrometers: a good energy resolution is obtained at the price of low intensity and small angular acceptance. Moreover the incoherent x-ray scattering cross section, although always very small, when using soft x-rays is further reduced because the dominant de-excitation channel is the non-radiative Auger decay. The main limitation is thus from signal intensity issues: only very recently did a combined band width better than 1 eV become available [5, 6], because previously the high resolution instruments could not be exploited at the best of their capabilities due to the insufficient count rate. In the last 10 years interesting results on 3d transition metal systems were indeed obtained in all those cases where energy resolution was not crucial both in RIXS [7, 4, 8, 9] and in resonant emission spectroscopy [10, 11], but only now is $L_{2,3}$ RIXS becoming an effective tool in the study of local electronic excitations thanks to the advances in the x-ray sources and optics in the synchrotrons (higher flux, better focusing of the monochromatic beam onto the sample) and in the x-ray CCD detectors. On the other side, at the $M_{2,3}$ edges (25–80 eV) the instrumental energy resolution is usually better than at the L edges, but an unfavourable ratio of the elastic/inelastic scattering cross sections has drastically limited the number of successful M edge RIXS measurements [12, 13]. This scarcity of published results has probably been due to the lack of VUV/soft x-ray beam lines optimized for RIXS as performed below 100 eV: recent results obtained at the M edge on NiO [13] open new perspectives at the M edges as well.

In this paper we present a set of high quality RIXS data measured across the Ni L_3 edge in NiO, with a measured energy band width of 0.55 eV (combined). The interpretation of the experimental data is made at three levels: the textbook model based on the Sugano–Tanabe diagrams for crystal field dd excitations; the simulation of the RIXS spectra using an atomic model with crystal field, spin–orbit interaction and inter-atomic (super-) exchange interaction; and the simulation of the spectra using a more sophisticated Anderson impurity Hamiltonian, including the hybridization of the 3d states with the O 2p electrons.

2. The experimental data and their basic interpretation

The spectra were measured at the beam line ID08 of the European Synchrotron Radiation Facility (ESRF) in Grenoble, using the AXES spectrometer [14] and its dedicated monochromator [15]. Thanks to a new variable line spacing (VLS) plane grating (1400 grooves mm^{-1}) the resolving power of the monochromator was recently increased ($E/\Delta E$ better than 3000 over the whole energy range going from oxygen K edge at 530 eV to the Cu L edges at 950 eV). The spectrometer resolution was also improved by installing a $13.5 \times 13.5\ \mu m^2$ pixel CCD camera [16] directly illuminated for the maximum efficiency: the 2400 groove mm^{-1} VLS spherical grating was originally designed to have the focal plane roughly perpendicular to the exit arm in an off-Rowland geometry, in order to avoid detection problems with CCD detectors. At present AXES in itself reaches the target resolving power of 2000 originally established. These figures are confirmed by the test measurements made recently: the full width at half maximum (FWHM) of the elastic peak is 620, 550, 480 and 320 meV at the Cu, Ni, Co and Mn L_3 edges respectively, meaning a combined resolving power better than 1500 for all the heavy 3d transition metals. The beam line source is a double APPLE II undulator [17] producing ~100% polarized (circular, linear horizontal, linear vertical) x-rays.

NiO has a rock-salt cubic structure, so that Ni ions occupy octahedral sites. Nominally Ni and O are divalent (Ni^{2+}, $3d^8\ 4s^0$; O^{2-}, $2p^6$) although it was clearly demonstrated that the

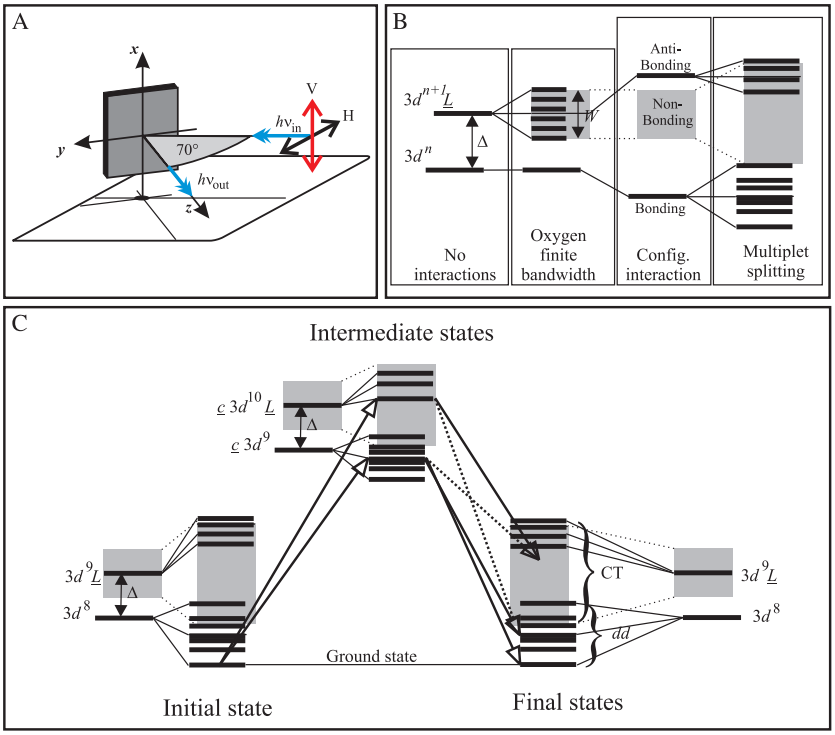

Figure 1. Panel (A): the experimental geometry used in the RIXS experiment. Panel (B): a schematic representation of the atomic model with configuration interaction used to describe the electronic structure of NiO in the ground and excited states; Δ is the charge transfer energy, W is the O 2p bandwidth, and $n = 8$ and 9 for the initial/final and intermediate states respectively; see the text for further details. Panel (C): scheme of the L_3 RIXS process in a total energy representation; the first transition is dictated by the incident photon energy and the second transition; the de-excitation transitions can lead to the ground state (elastic peak), to dd or to charge transfer excited states.

hybridization between Ni 3d and O 2p states leads to a $3d^{\sim 8.2}$ population [18]. The spectra were measured at room temperature on a single crystal, cleaved in air: below the Néel temperature ($T_N = 523$ K) the sample is antiferromagnetic and split in small domains where the spin moments are parallel/antiparallel to any of the eight equivalent $\langle 112 \rangle$ directions [19, 20]. The experimental geometry is sketched in figure 1, panel (A). The scattering angle was 110° in the horizontal plane. The incident beam was impinging at 20° from the (001) surface and the analysed radiation was along the [001] direction, normal to the sample surface. The polarization of the incident radiation was set either lying in the scattering plane (H-pol for horizontal polarization) or perpendicular to the scattering plane (V-pol for vertical polarization). The scattered radiation degree of polarization was not detected. We notice here that the H-pol and V-pol cases correspond to the depolarized and polarized geometries of [21, 22].

Figure 2 shows one set of data taken across the Ni L_3 edge with a measured combined resolution of 750 meV and V-pol. The labels for the excitation energies (C to K) indicate 1 eV steps, and the reference point was always the L_3 peak (point F). Below $L_3 + 0.5$ eV we measured one spectrum every 0.25 eV, above one every 0.5 eV. The absorption spectrum in the lower left panel of figure 2 was measured in total electron yield with exactly the same settings used for RIXS. The RIXS spectra are as measured (after the necessary conversion from the units of the CCD detector read-out system to number of photons and from the pixel position

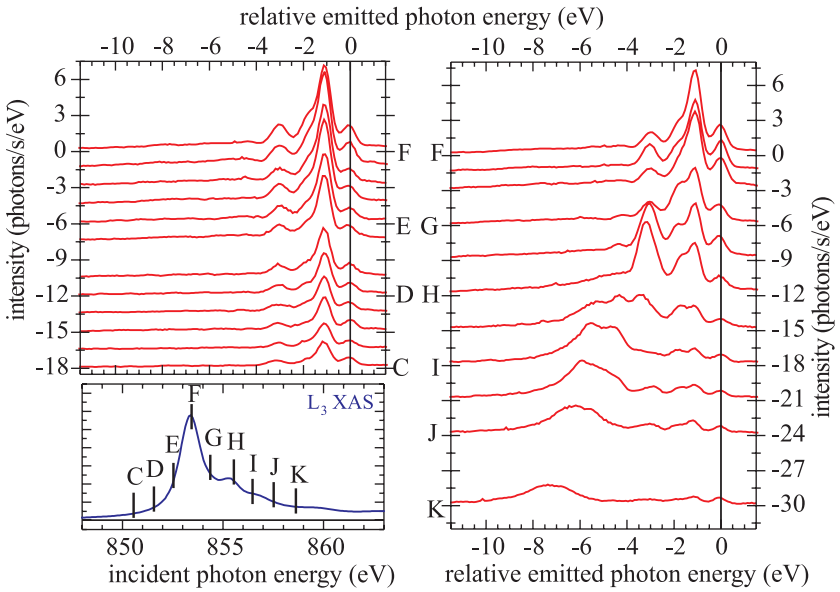

Figure 2. Experimental Ni L_3 RIXS spectra measured with 750 meV combined resolution. The lower left panel shows the Ni L_3 absorption spectrum measured with the same incident energy resolution and the labels of the excitation energies used for the RIXS spectra. The polarization of the incident photons was V-pol, i.e. perpendicular to the scattering plane.

to the photon energy): the sampling step is 93 meV and on the peak at least 500 counts/point were accumulated for each spectrum. Most of the shown spectra were measured in 8 min each. In the same session the H-pol spectra were measured as well (not shown here). The spectra in figures 3, 4 and 6 were measured under the same conditions but with better resolution (FWHM 550 meV combined) and finer sampling step (67 meV) after the replacement of the CCD detector with one of smaller pixel size.

Our spectra are consistent with those measured recently by Ishii *et al* [23] and by Magnuson *et al* [24], but the better energy resolution and statistical quality allow us to unravel a more detailed spectral structure. Below the point F + 0.5 eV the spectral shape evolves very little and five structures can be recognized: the elastic peak, a main peak around −1.1 eV, one shoulder at −1.8 eV, one peak at −3.0 eV and a long tail below −4 eV. Above the main peak the spectra change shape at every excitation energy, but the position of the peaks is almost constant for all the features between −4 eV and 0. Moreover, we can recognize another peak at −4.2 eV in the spectra from G to I. From excitation H to K the low energy tail is increasingly more intense and disperses towards lower energies: this behaviour is typical of x-ray fluorescence emission, whereas the genuine Raman-like parts of the spectra remain at fixed energy with respect to the elastic peak. The transition from Raman-like to fluorescence-like emission spectra has been studied before for NiO in photoemission [25, 26] and x-ray emission [27]: the onset of the fluorescence-like behaviour is usually related to the width of the bandgap in insulators and semiconductors. As we shall discuss more extensively below and as pointed out by Matsubara *et al* [22], the transition from Raman-like to fluorescence-like behaviour is complicated by the presence of charge transfer excitations, which have a mixed local–nonlocal character, so that for the moment we leave incomplete the interpretation of the spectra H to K and we concentrate our attention on the pure Raman part of the spectra.

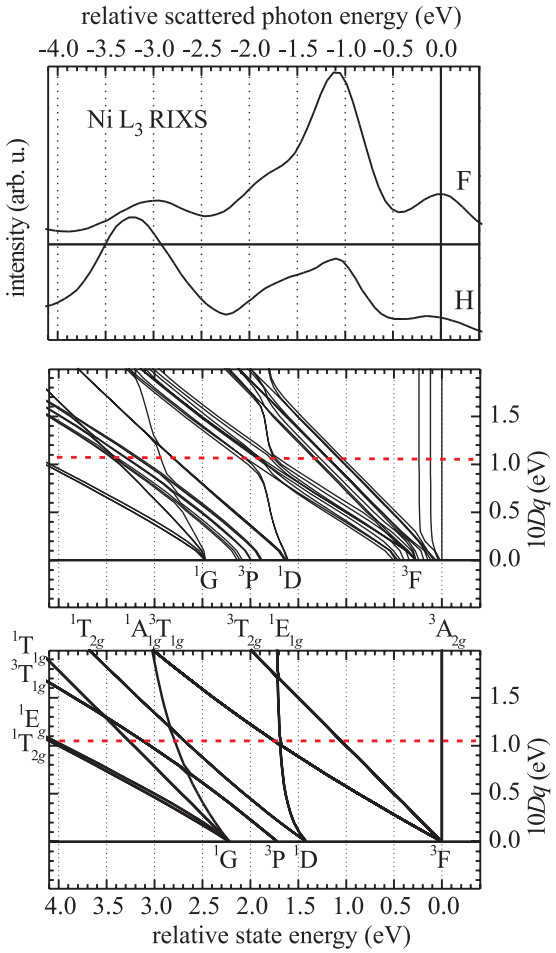

Figure 3. Bottom panel: the Sugano–Tanabe diagram for the $3d^8$ configuration in a octahedral crystal field calculated with a reduction of 0.7 of the Slater integrals, no 3d spin–orbit interaction and no inter-atomic exchange interaction. Middle panel: the Sugano–Tanabe diagram calculated with $\zeta_{3d} = 84$ meV, $H_{exch} = 120$ meV. Top panel: the experimental spectra measured with 550 meV energy resolution with excitation on the main peak (F) and on the satellite (H) of the L_3 absorption spectrum, using V-pol. The main spectral features can be directly related to the dd excitations given in the Sugano–Tanabe diagrams for $10Dq = 1.05$ eV marked by a dashed line in the bottom and middle panels.

For the part of the spectra going from −4 eV to 0 we can directly refer to the models used traditionally in optical spectroscopy, and in particular the crystal field calculations. In fact, through the double radiative transition $2p \rightarrow 3d \rightarrow 2p$ the scattering process gets localized on one Ni ion, resulting in $3d^n \rightarrow 2p^5 3d^{n+1} \rightarrow [3d^n; 3d^{n*}; 3d^{n+1}\underline{L}]$, where n is the actual 3d occupation number and $\underline{L}$ indicates a ligand hole. $3d^{n*}$ stands for a final state where n has not changed but the 3d electrons have been re-distributed among the available orbitals: these are the dd excitations. The new configuration is at higher energy with respect to the ground state and the energy difference is detected as energy loss in the x-ray scattering process. $3d^n$ indicates the ground state (elastic peak), and $3d^{n+1}\underline{L}$ are the charge transfer excitations.

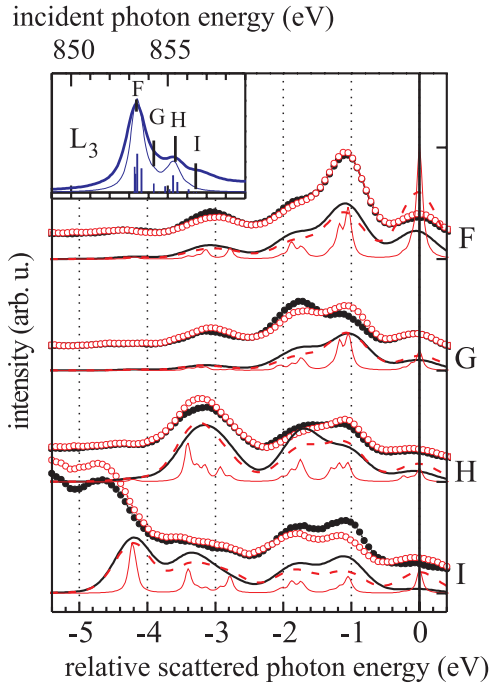

Figure 4. The spectra calculated with the single-configuration atomic model with crystal field are compared with the experimental ones for both V-pol and H-pol polarizations at four selected excitations. Colours and symbols: red/open circles/dashed lines are for V-pol; black/full circles/solid lines are for H-pol. Lines are calculated; circles are measured. Thin lines are with 100 meV FWHM Lorentzian broadening in the RIXS final state, thick lines are with 500 meV FWHM Gaussian broadening in the RIXS final state. In the inset the comparison of the absorption spectra. The thick line is measured; the thin line is calculated. See the text for details.

In figure 1, panel (B) shows a scheme of the atomic picture used in the following to describe the RIXS process. The cartoon can apply to the initial and final states ($n = 8$) or to the intermediate state ($n = 9$), where the covalency of the Ni–O bond in the solid is taken into account by the interaction between two atomic configurations, having n and $n + 1$ 3d occupancy at the Ni sites. The distance between the two *non-interacting* configurations is indicated by Δ, often called charge transfer (CT) energy. The $3d^{n+1}\underline{L}$ configuration has a finite bandwidth W, because the O 2p states are known to have a delocalized character. If then the actual overlap between the two configurations (which depends on the hybridization of Ni 3d and O 2p states) is taken into account we have three configurations, two of mixed character (bonding and anti-bonding) whose centers of mass are at a distance greater than Δ [28, 29, 22], and one (non-bonding) whose energy is negligibly altered by the hybridization. Despite their mixed nature the two interacting configurations still have main $3d^n$ and $3d^{n+1}$ character and they have a localized nature. The non-bonding states have also mainly $3d^{n+1}$ character (they are charge transfer states) but they are delocalized and they form a continuum. In $3d^0$ systems like Ti in TiO_2 the anti-bonding and the non-bonding states are well separated in energy and they can be recognized in the RIXS spectra [29, 21, 30]. In NiO the anti-bonding states are probably indistinguishable from the non-bonding band [22] so in the following we will ignore them and we will refer more generally to the charge transfer states as a collection of states distributed over a quasi-continuous energy range. Finally, we consider the intra-atomic Coulomb interaction

(including the crystal field), which splits the two configurations into multiplets. In figure 1, panel (C) a summary of the possible transitions is given. In the initial state the system is in the lowest energy state, i.e. the ground state. Upon absorption of one x-ray photon the system reaches the intermediate state: the energy and polarization of the absorbed photon determine what state is actually chosen. The emission of a photon (of given polarization and energy) leads to the final state, to be "chosen" among all the possible ones. In general all the transitions are possible, but with different probabilities. In particular if the intermediate state has mainly $3d^9$ ($3d^{10}\underline{L}$) character the final state will more likely have $3d^{8*}$ ($3d^9\underline{L}$) nature, i.e. it will be of dd (charge transfer) type. In this way the incident photon energy can be used to enhance the dd or the CT excitations in all those cases where the two configurations are sufficiently separated in energy in the intermediate state. This happens in NiO, but could be different in other systems (manganites, cobaltates, nickelates) known to have a smaller effective separation between $3d^n$ and $3d^{n+1}\underline{L}$ configurations. Finally, it is important to notice that in the intermediate state the core hole potential reduces the 3d–2p hybridization, implying a smaller effective separation between $3d^n$ and $3d^{n+1}\underline{L}$ configurations.

Within the given framework we can thus decide to separately analyse the dd and CT excitations. As shown later on, the dd excitations can be well described by a crystal field model where only the $3d^8$ atomic states are placed under the static crystal field, but the influence of the interaction with the $3d^9\underline{L}$ configuration can effectively be taken into account by renormalizing the crystal field parameter $10Dq$ and the Slater integrals. This is why we start our analysis from the dd excitations.

The dd excitations of NiO were studied with optical absorption already in the 1950s [31] and the basic assignments were made on the basis of crystal field model calculations, where a single ion, with integer n, is placed in a non-spherical electrostatic field due to the neighbours [32, 33]. The crystal field effect is added to the intra-atomic effects (electron–electron repulsion, spin–orbit interaction) and to the magnetic interaction with the neighbouring Ni ions (inter-atomic exchange interaction) [34, 35]. For the octahedral symmetry (probably the most common in the solids) the calculations of the crystal field effects were made systematically for all the 3d occupation numbers, from 2 to 8 (1, 9 and 10 are trivial), and are usually known as Sugano–Tanabe diagrams [36, 32].

In figure 3, the bottom panel shows the Sugano–Tanabe diagram calculated with the Cowan code and later modifications by Thole *et al* [34, 37, 38] for a $3d^8$ configuration. The pure atomic terms (^{3}F, ^{1}D, ^{3}P, ^{1}G) are split into a variety of terms indicated by the group theory derived notation in O_h (octahedral) symmetry. In that type of diagram the energy of each configuration is plotted as a function of the $10Dq$ parameter, that is the energy separation between the singly occupied e_g (x^2–y^2, z^2 symmetry) and t_{2g} (xy, yz, zx) orbitals. So in Ni^{2+} the ground state (energy equal to zero) is a triplet ^{3}F in spherical symmetry and a triplet $^3A_{2g}$ in the presence of a crystal field, corresponding to a $t_{2g}^6e_g^2$ occupation. The first dd excitation (for $10Dq < 1.5$ eV) is the $^3T_2$ ($t_{2g}^5e_g^3$): the energy difference is exactly equal to the value of $10Dq$, as one electron has moved from a t_{2g} to an e_g orbital. In this way the value of the effective $10Dq$ for NiO has been known for many years, from the measurement of the lowest energy dd excitation: for example already in 1959 Newman and Chrenko could estimate $10Dq = 1.13$ eV from optical absorption spectra [31]. By comparing the spectra F and H with the Sugano–Tanabe diagram (figure 3(c)) we find once again that $10Dq \approx 1.1$ eV, in agreement with the literature. Up to now dd excitations have been studied either by optical absorption [31, 20] or electron energy loss spectroscopy (EELS) [39–41]: with all techniques the energy of the excited states is the same and can be theoretically estimated [42], but the transition cross-sections are very much harder to calculate in optical absorption and EELS than

in RIXS. RIXS results from two dipole-allowed transitions are easily simulated with atomic calculations: this is a distinct advantage that largely compensates the lower energy resolution of RIXS with respect to other spectroscopies addressing dd excitations. Moreover the spectra presented here demonstrate that the L_3 RIXS spectra can be interpreted directly in a way very similar to optical spectroscopies despite the presence of core holes in the intermediate state: the determination of the crystal field parameter $10Dq$ using RIXS remains a demonstration in the case of NiO but it can be of high interest for many other systems where optical spectroscopies are not appropriate or give ambiguous results.

In 3d transition metal systems other interactions play a central role in the determination of the electronic structure: the 3d spin–orbit interaction and the exchange interaction. In the central panel of figure 3 the Sugano–Tanabe diagram was calculated taking into account both interactions (spin–orbit: $\zeta_{3d} = 84$ meV; inter-atomic exchange integral: $H_{exch} = 120$ meV): the number of non-degenerate states grows considerably and the correspondence to the measured spectra becomes less direct. We can notice that the singlet states are almost unaffected, whereas the triplet states are split into a dense multiplicity of different states. The ground state has now two satellites at 120 and 240 meV, corresponding to the two possible magnetic excitations of the $S = 1$ atomic spin moment. This is the energy required to break the local magnetic arrangement with respect to the local magnetic order of the rest of the crystal. In $3d^8$, the $^3A_{2g}$ term is negligibly affected by the 3d spin–orbit interaction, which is not the case of the $^3T_{1g}$ term: it is a fortunate coincidence that the ground state in Ni^{2+} allows such a direct measurement of the exchange interaction. The same does happen for example for $3d^5$ but not for $3d^7$. For Ni^{2+} the original suggestion to use high resolution RIXS to get an estimate of H_{exch} came from de Groot *et al* [43]. Our spectra at L_3 are still not resolved enough in energy but the measurement should become possible with the higher performing RIXS instrumentation to be built in the near future. The $H_{exch} = 120$ meV was chosen in consideration of the analysis done in [13] on the M edge RIXS spectra, of the optical absorption spectra of [31] showing very clearly the two magnon excitation at 240 meV, and of the neutron scattering measurements of [19].

From figure 2 it appears that when exciting at the 2 eV satellite of the L_3 main peak in the RIXS spectrum the peaks at -1.8 eV and at -3.3 eV are enhanced with respect to the -1.1 eV peak as compared to the F excitation (main L_3 peak). The satellite in the absorption corresponds to a spin-flip excitation, i.e. the intermediate state has dominant singlet character (although in the $2p^53d^9$ configuration spin is not a good quantum number due to the strong 2p spin–orbit interaction). The final state of RIXS is thus dominated by the singlet final states, whose energies correspond to the main features in the H spectrum shown in figure 3 [23].

The diagrams of figure 3 can also be used to estimate the effective value of the Slater integrals. In fact, the dd excitations related to the ^3F atomic term are not influenced by the intra-atomic Coulomb and exchange interactions, whereas the energy of the ^1D, ^3P and ^1G and derived states mainly depend on those interactions. The values calculated for the isolated atom using the Hartree–Fock–Slater method are usually not satisfactory for the solids, mainly because the hybridization with the neighbouring atoms leads to an effective non-integer 3d population. The normal practice is to reduce the Slater integrals. Even for the isolated atom, the Slater integrals are rescaled to 80–85% of those calculated by a standard Hartree–Fock program to account for intra-atomic configuration interaction, but in the crystal field model they should be further reduced to account for the hybridization effect (inter-atomic configuration interaction). These reduction factors are empirical ones and a real justification for this 'magic' number has never been given [44]. With the RIXS spectra the adjustment of the reduction factor when using a pure $3d^8$ configuration is probably easier than with any other spectroscopic technique. In fact, $10Dq$ and the Slater integrals act on different parts of the spectra: in our

case the first peak at −1.1 eV determines the optimum $10Dq = 1.05$–1.10 eV and the peak at −3.2 eV fixes the Slater integrals to 70% of their atomic value.

All the considerations of this section were made without the help of simulated RIXS spectra. In order to take full advantage of the second-order electric dipole allowed RIXS process the calculation of the spectral intensities is necessary, so that the assignment of the character of the excitations can be made more precisely.

3. Calculations: single ion with crystal field model

In figure 4 we present the RIXS spectra calculated within the single-ion with crystal field model already introduced in the previous section [34, 45]. The single $3d^8$ configuration is considered and the $3d^8 \rightarrow 2p^5 3d^9 \rightarrow 3d^8$ process is computed for all the possible terms in the D_{4h} symmetry (undistorted octahedral site with spin moment along the z axis). The cross section is calculated following the Kramers–Heisenberg formula for the same scattering set-up used in the experiment: 110° scattering angle, incidence direction at 20° from one of the main axes, emission along one of the axes, linearly polarized incident photons oriented V-pol or H-pol following the definition of section 2. In order to take into account the multi-domain magnetic structure we calculated the spectra for the three inequivalent orientations having the atomic moment perpendicular to the scattering plane, or in the scattering plane both along the emission direction or at 20° from the incidence direction. The shown spectra are the arithmetic average of the three cases. For each incident polarization the intensities were summed over the two independent polarizations of the scattered photons. The lifetime Lorentzian broadening in the intermediate and final states were set to 300 and 100 meV respectively. The final RIXS spectra are presented both with no broadening (thin lines) and after a Gaussian 500 meV FWHM convolution to simulate the instrumental band width. With the same parameters we calculated the L_3 absorption spectrum shown in the inset. The parameters were $10Dq = 1.05$ eV, $H_{\mathrm{exch}} = 120$ meV, Slater integral reduction 70% resulting in the Racah parameters $A = -0.590$ eV, $B = 0.114$ eV, $C = 0.421$ eV, spin–orbit parameter $\zeta_{3d} = 84$ meV corresponding to 210 meV single particle spin–orbit splitting. Clearly the charge transfer excitations are absent from the calculated spectra as the only possible final states included in the calculations have a $3d^8$ configuration.

The comparison shown in figure 4 for the F, G, H and I excitations and for the absorption is rather satisfactory, since the calculated spectra are in good agreement with the measured ones in the whole −4 to 0 eV range where dd excitations dominate. Also the linear dichroism, i.e. the effect of rotating the incident polarization vector from V-pol to H-pol, is well reproduced. The main discrepancy is in the intensity of the elastic peak, which is influenced in the experiment by the self-absorption of the scattered photons and by other scattering processes (Rayleigh scattering). The shown agreement can be obtained only by averaging over the three magnetization orientations as described above. In case H the unbroadened spectrum with V-pol presents in the most evident way the −120 and −240 meV satellites of the elastic peak that were assigned in section 2 to the atomic moment flipping. These peaks although less evident are present for the other excitations and for the H-pol excitation as well (not shown).

These calculated spectra confirm that dd excitation, thanks to their local character, can be studied effectively with L_3 RIXS and can be interpreted within a crystal field model: as crystal field parameters are sensitive to the local crystalline structure, RIXS can be effectively used to study local distortions in solids and their influence on the 3d electronic structure. The use of linear polarization orientation and of single crystals can further help in recognizing the symmetry of the dd excitations.

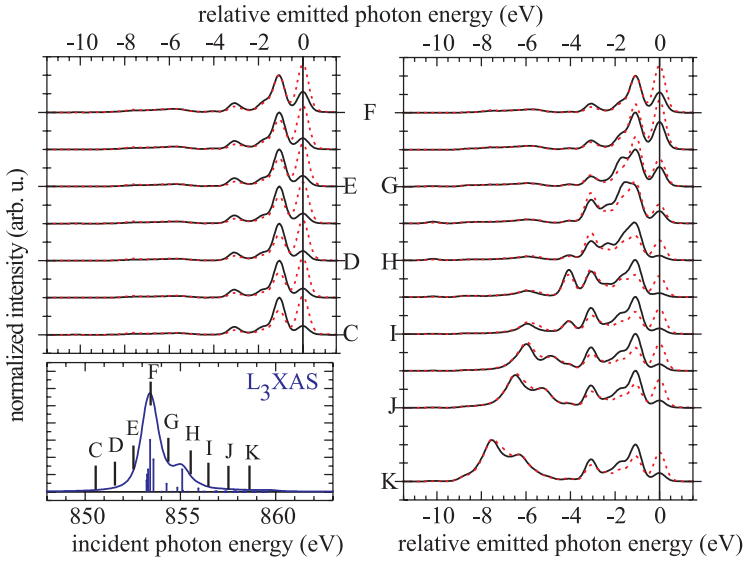

Figure 5. The RIXS and absorption spectra calculated with the Anderson impurity model at the same excitation energies used in the experiment. Colours and symbols: red dashed lines are V-pol, black solid lines are H-pol. The spectra were broadened with a 500 meV FWHM Guassian in the final state.

Table 1. Parameters used in the Anderson impurity model calculations of the absorption and RIXS spectra of figures 5 and 6.

Parameter	Value	Description
$10Dq$	0.5 eV	Energy difference of e_g and t_{2g} states in Ni before hybr.
Δ	3.5 eV	Charge transfer energy ($E(3d^9\underline{L}) - E(3d^8)$)
U_{dd}	7.2 eV	Coulomb repulsion on Ni site: the energy of adding one 3d electron
U_{dc}	8.0 eV	Coulomb attraction on the 3d by the Ni 2p core hole
$V(e_g)$	2.2 eV	Hybr. integral between Ni 3d and O 2p states with e_g symmetry
$V(t_{2g})$	−1.1 eV	Hybr. integral between Ni 3d and O 2p states with t_{2g} symmetry
W	3.0 eV	Width of the O 2p band
	85%	Slater integral rescaling
R_c	0.8	Hybr. rescaling for the 3d shell contraction due to core hole
$1/R_v$	1/0.9	Hybr. rescaling for the 3d shell expansion due to addition of one 3d electron

4. Calculations: Anderson impurity model

In figure 5 we present the spectra calculated with the Anderson impurity model considering a full multiplet structure extensively presented by Matsubara *et al* in [22] and previously used by Magnuson in [24] for NiO. The calculation was made in O_h symmetry, with no inter-atomic exchange interaction. The parameters used for the spectra of figure 5 are summarized in table 1.

The model is similar to that of figure 1, panel (B), where Δ and W were already introduced. It has to be noticed that the finite bandwidth W is here approximated by six discrete states equally spaced within a W energy range. The 3d–2p hybridization integrals are different for the states of different symmetry $V(e_g)$ and $V(t_{2g})$, due to the different overlap of Ni 3d and O 2p orbitals in the various cases. The model takes into account three interacting configurations: $3d^8$, $3d^9\underline{L}$, and $3d^{10}\underline{L}^2$. The spin–orbit parameters and the Slater integrals for the 3d states are

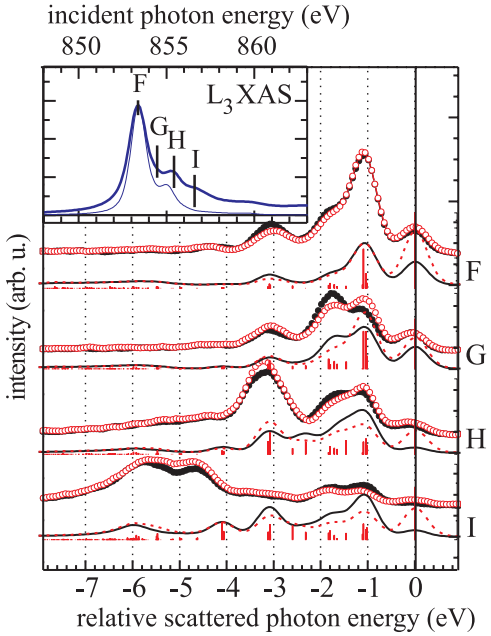

Figure 6. The spectra calculated with the Anderson model are compared with the experimental ones for both V-pol and H-pol at four selected excitations. Colours and symbols: red dashed lines are V-pol, black solid lines are H-pol. Solid lines are calculated; circles are measured. Bars indicate the energy and intensity of final states. Thick lines are with 500 meV FWHM Gaussian broadening in the RIXS final state. In the inset is the comparison of the absorption spectra. See the text for details.

calculated with a Hartree–Fock atomic code. The spectra were calculated using the Kramers–Heisenberg formula for the same scattering geometry as used in the experiment and using a 300 meV Lorentzian lifetime in the intermediate state. The spectra in figure 5 were convoluted with a 50 meV Lorentzian and a 550 meV FWHM Gaussian.

The overall spectral shapes, excitation energy dependence and polarization dependence for the dd excitation part are close to the experimental data as shown in figure 6. As expected, the dd excitation spectra by the present calculation are almost the same as those by the crystal field model calculation in section 3: the spectra calculated with a single $3d^8$ configuration but with a renormalized $10Dq$ and Slater integrals and those with a triple interacting configuration are both remarkably close to the experimental spectra. In addition here we have the presence of excitations in the -10 to -4 eV range: these excitations become increasingly important for the I, J and K cases, and have dominant charge transfer character. Also, the absorption spectrum is more extended than for the calculations of figure 4, where no intermediate states are present above excitation I. The calculated spectra above excitation H show no evolution of the dd part and a dispersing double peak in the CT part (figure 5), in agreement with the general trend of the experimental spectra (figure 2). We notice here that the charge transfer peaks show an apparent fluorescence-like behaviour, which comes from the finite band width of the oxygen 2p states. Nevertheless these (calculated) peaks are genuine RIXS peaks, as shown in [22]: for high enough excitation energy (above point K but below the L_2 edge) the charge transfer excitations stay at constant energy loss and eventually become negligibly weak. There the normal fluorescence decay channel dominates, as can be seen in [23] and as highlighted by Matsubara *et al* [22]. This transition from Raman scattering to fluorescence is

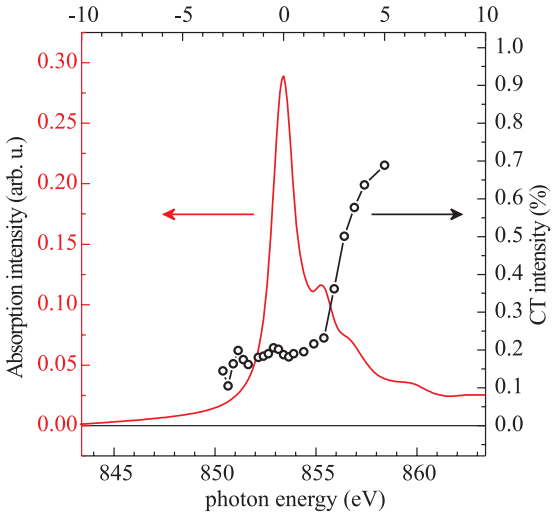

Figure 7. The onset of the charge transfer excitation spectral weight as a function of the incident energy. Up to 2.5–3.0 eV above the main L_3 peak only 20% of the RIXS spectral intensity has charge transfer character (energy loss greater than 5 eV). The charge transfer/fluorescence becomes dominant above $L_3 + 4.0$ eV.

very complicated. We notice that the final state of an RIXS scattering with CT excitation and of a non-resonant fluorescence emission are very close in energy because in both cases the energy difference between the incident and emitted photons is delocalized, to the solid through the O 2p band in the former and to the photoemitted electron in the latter case. So in the two cases the emission spectrum appears at constant emitted energy. The CT RIXS and non-resonant fluorescence differ mainly for the local 3d configuration ($3d^9$ and $3d^8$ respectively): the two multiplets are different but the spectra appear at similar emission energies. Separating the two contributions in the experimental spectra is probably very difficult.

In figure 7 we show the fractional spectral weight of the CT RIXS over the total RIXS experimental spectrum as a function of the excitation energy in the case of V-pol excitation. We chose to consider as CT RIXS all the intensity in the -20 to -5 eV energy range, although this can include a contribution from fluorescence. We can see that the onset of the CT/fluorescence is around 3.5 eV above the main L_3 absorption peak, indicating that in the intermediate state the effective distance between the lowest $3d^9$ state and the lowest $3d^{10}\underline{L}$ state is around 3.5 eV. On the other hand we know from the RIXS spectra and from the calculations that in the initial/final state the lowest $3d^9\underline{L}$ state lies around 5 eV above the ground state. This indicates that the 2p core hole decreases the distance between dd and CT states. In [26] the transition from Raman- to Auger-like behaviour of resonant photoemission peaks across the L_3 peak had been already addressed. In that case the authors made a direct link between the onset of the Auger-like behaviour (3.5 eV above the threshold) and the bandgap of NiO.

A final remark has to be devoted to the value of $10Dq$. As reported in table 1 in the Anderson impurity model calculations the optimum value for $10Dq$ is 0.5 eV, whereas the first dd excitation is at 1.1 eV and consequently in the single configuration calculations we have used $10Dq = 1.05$ eV. The difference comes from the hybridization integrals $V(e_g)$ and $V(t_{2g}) = -1/2V(e_g)$ and from the initial energy difference between $3d^8$ and $3d^9\underline{L}$ states that are different for the e_g and the t_{2g} states. Thus the $10Dq$ splitting assigned to the non-interacting 3d states has to be smaller when using interacting configurations. For similar

reasons the reduction of the Slater integrals is weaker for the Anderson impurity model than for the single-configuration calculations. There again the reduction is a way of accounting for the interaction with the neighbouring atoms: when the 3d–2p hybridization is explicitly introduced the 'blind' intervention on the Slater integrals can be weakened.

The role of 3d–2p hybridization on the optimized values of theoretical parameters has been a matter of important discussions already in the past, and what we are adding here is the clear observation that RIXS can be used to compare, in a transparent way, the parameters found in the various models. In fact, the crystal field model has been demonstrated to be extremely effective for the interpretation of the optical absorption spectra via the Sugano–Tanabe diagrams [36], but already in the 1960s the role of covalency in the determination of $10Dq$ was a central issue [47]. On the other hand core level spectroscopies, at the beginning of the 1980s, motivated the use of configuration interaction models in order to account for the experimental findings in x-ray photoemission and x-ray absorption spectroscopy. Then cluster model [42] and impurity model [28, 48] calculations proved to be necessary to adequately reproduce the photoemission and absorption spectra of NiO. In the presence of a core hole in the final state the choice of $10Dq$ was there either very different (1.5 eV) [48] from the generally accepted values, or neglected at all [28], whereas valence photoemission was demonstrated to be compatible with an e_g–t_{2g} atomic splitting of the order of 0.5 eV when using a cluster model [42]. As already mentioned, the role of hybridization in the determination of the 3d energy levels has already been discussed in the cited articles. Moreover, in [42] it was found that, for valence photoemission, in a simple crystal field model one should use $10Dq \simeq 1.1$ eV and reduce the Slater integral to 70% of their value for an isolated atom, as we find too. What we are showing in the the present paper is that, to a very high degree of accuracy, the parameters optimized for the ground state and for low energy electronic excitations (those of valence photoemission or optical spectroscopies) are also valid for RIXS, in spite of the presence of a core hole in the intermediate state. The peculiarity of RIXS is thus the ability of exploring the ground state properties by combining the selectivity of resonant core level techniques and the transparency of optical spectroscopy.

5. Conclusions

We have presented high resolution L_3 RIXS spectra of NiO and analysed them at various levels of complexity. Recently we succeeded in increasing the efficiency and resolving power of our RIXS apparatus for soft x-rays so that excellent spectra can be recorded in a few hours at most of the 3d transition metal $L_{2,3}$ edges. The quality of the experimental spectra reveals a rich spectral structure, dependent on the incident photon energy and polarization orientation: this valuable information has to be conveniently exploited beyond the pure phenomenology. The interpretation of L_3 RIXS in strongly correlated electron systems is relatively straightforward when working in an atomic scheme. Then the spectral features can be easily separated into dd and CT excitations, which in NiO lie farther or closer than approximately 4 eV from the elastic peak respectively. The Sugano–Tanabe diagrams can help in assigning the dd excitations even in the absence of any simulations of the spectra: a relatively precise estimate of the effective $10Dq = 1.05$ eV can then be made in the cubic systems. Using a single atomic configuration and a crystal field model the RIXS spectra can be fully simulated in their dd part, adding further insight in terms of exact assignment of the final state symmetry. The simulated spectra can be used to refine the calculation parameters: we obtained in a very direct way that the Slater integral reduction factor has to be 70%. Finally, more sophisticated models (cluster model, Anderson impurity model) can be used for simulating the spectra: there other important parameters like the charge transfer energy $\Delta = 3.5$ eV and the 3d–2p hybridization integrals

can be deduced in a very direct way when optimizing both the dd and CT parts of the RIXS spectra, together with the absorption spectrum. L_3 RIXS is not just "another" resonant x-ray spectroscopy: it shares with optical spectroscopy a wide known framework (the crystal field model), whilst exploiting the power of chemical selectivity intrinsic to all x-ray spectroscopies.

Great efforts are currently being made at various synchrotron radiation facilities to further improve the resolution of RIXS spectra. This gain in resolving power will serve to measure even richer and finer details in the local electronic and magnetic excitations in solids: for example, a direct determination of the inter-atomic exchange interaction will be soon at hand using L_3 RIXS. At the same time $M_{2,3}$ RIXS is also growing on the experimental side: the very small cross sections have been up to now the main obstacle to a more extensive use, despite a much more favourable energy resolution [13]. One other difference between L and M edge RIXS is the presence and almost absence of the CT excitations in the final state, respectively. There are probably various factors contributing to this difference, among them the different hybridizations in the intermediate state and different resonant enhancements in the excitation. In fact, in the intermediate state the 2p core hole attraction is stronger that that of a 3p hole, leading to a higher transition probability towards the charge transfer configuration in the intermediate state. The p lifetime broadening of the intermediate state is smaller at the L than at the M edges, leading to sharper and stronger resonances also when exciting the CT intermediate states, as suggested in [46]. In all cases (M and L edge RIXS) a further gain in resolving power is desirable: the lifetime broadening of the intermediate state does not limit the resolution of the low energy electronic excitations in the final state. Moreover, the intrinsic lifetime broadening of the dd excitations is often much smaller than the present instrumental energy resolution in RIXS experiments. For NiO this is demonstrated in the optical absorption spectrum shown in [20]: peaks separated by a few tens of meV are clearly resolved. Reaching such a high degree of detail in RIXS is an ambitious technical challenge that can be realized using dedicated beam lines and newly designed spectrometers.

Acknowledgments

The experimental data were taken at the ESRF using the AXES instrumentation within the AXES (Advanced X-ray Emission Spectroscopy) contract, between the ESRF and the INFM/CNR. The technical help of G Retout is gratefully acknowledged. LB, CD and GG are deeply indebted to M Grioni for stimulating discussions. The authors would like to thank Professor T Uozumi for providing us with his computer program in our RIXS calculation with the Anderson impurity model.

References

[1] Hill J P, Kao C-C, Caliebe W A L, Matsubara M, Kotani A, Peng J L and Greene R L 2003 *Phys. Rev. Lett.* **80** 4967
[2] Kao C-C, Caliebe W A L, Hastings J B and Gilet J-M 1996 *Phys. Rev.* B **54** 16361
[3] Shukla A, Rueff J-P, Badro J, Vanko G, Mattila A, de Groot F M F and Sette F 2003 *Phys. Rev.* B **67** 081101
[4] Harada Y, Okada K, Eguchi R, Kotani A, Takagi H, Takeuchi T and Shin S 2002 *Phys. Rev.* B **66** 165104
[5] Ghiringhelli G, Brookes N B, Annese E, Berger H, Dallera C, Grioni M, Perfetti L, Tagliaferri A and Braicovich L 2004 *Phys. Rev. Lett.* **92** 117406
[6] Ghiringhelli G, Matsubara M, Dallera C, Fracassi F, Tagliaferri A, Brookes N B, Kotani A and Braicovich L 2005 submitted
[7] Butorin S M, Guo J-H, Magnuson M, Kuiper P and Nordgren J 1996 *Phys. Rev.* B **54** 4405
Magnuson M, Butorin S M, Guo J-H and Nordgren J 2002 *Phys. Rev.* B **65** 205106

[8] Braicovich L, van der Laan G, Ghiringhelli G, Tagliaferri A, van Veenendaal M A, Brookes N B, Chervinskii M M, Dallera C, De Michelis B and Dürr H A 1999 *Phys. Rev. Lett.* **82** 1566
[9] Taguchi M, Braicovich L, Borgatti F, Ghiringhelli G, Tagliaferri A, Brookes N B, Uozumi T and Kotani A 2001 *Phys. Rev.* B **63** 245114
[10] Kurmaev E Z, Moewes A, Butorin S M, Katsnelson M I, Finkelstein L D, Nordgren J and Tedrow P M 2003 *Phys. Rev.* B **67** 155105
[11] Yablonskikh M V, Yarmoshenko Yu M, Grebennikov V I, Kurmaev E Z, Butorin S M, Duda L-C, Nordgren J, Plogmann S and Neumann M 2001 *Phys. Rev.* B **63** 235117
[12] Kuiper P, Guo J-H, Såthe C, Duda L-C, Nordgren J, Pothuizen J J M, de Groot F M F and Sawatzky G A 1998 *Phys. Rev. Lett.* **80** 5204
[13] Chiuzbäian S G, Ghiringhelli G, Dallera C, Grioni M, Amann P, Wang X, Braicovich L and Patthey L 2005 *Phys. Rev. Lett.* submitted
[14] Dallera C, Puppin E, Fasana A, Trezzi G, Incorvaia N, Braicovich L, Brookes N B and Goedkoop J B 1996 *J. Synchrotron Radiat.* **3** 231
[15] Ghiringhelli G, Tagliaferri A, Braicovich L and Brookes N B 1998 *Rev. Sci. Instrum.* **69** 1610
[16] ROPER Scientific, Princeton Instruments PI-SX 2k
[17] Chavanne J, van Vaerenbergh P, Elleaume P and Gunzel T 2000 *Proc. EPAC 2000 (Vienna, Austria)* p 2346
[18] van Elp J, Eskes H, Kuiper P and Sawatzky G A 1992 *Phys. Rev.* B **45** 1612
[19] Hutchings M T and Samuelsen E G 1972 *Phys. Rev.* B **6** 3447
[20] Fiebig M, Fröhlich D, Lottermoser Th, Pavlov V V, Pisarev R V and Weber H-J 2001 *Phys. Rev. Lett.* **87** 137202
[21] Harada Y, Kinugasa T, Eguchi R, Matsubara M, Kotani A, Watanabe M, Yagishita A and Shin S 2000 *Phys. Rev.* B **61** 12854
[22] Matsubara M, Uozumi T, Kotani A and Parlebas J-C 2005 *J. Phys. Soc. Japan* **74** 2052
[23] Ishii H, Ishiwata Y, Educhi R, Harada Y, Watanabe M, Chainani A and Shin S 2001 *J. Phys. Soc. Japan* **70** 1813
[24] Magnuson M, Butorin S M, Agui A and Nordgren J 2002 *J. Phys.: Condens. Matter* **14** 3669
[25] Tjernberg O, Söderholm S, Karlsson U O, Chiaia G, Qvarford M, Nylén H and Lindau I 1996 *Phys. Rev.* B **53** 10372
[26] Finazzi M, Brookes N B and de Groot F M F 1999 *Phys. Rev.* B **59** 9933
[27] Braicovich L, Dallera C, Ghiringhelli G, Brookes N B, Goedkoop J B and van Veenendaal M A 1997 *Phys. Rev.* B **55** 15989
[28] Zaanen J, Westra C and Sawatzky G A 1986 *Phys. Rev.* B **33** 8060
[29] Idé T and Kotani A 2000 *J. Phys. Soc. Japan* **69** 1895
[30] Matsubara M, Uozumi T, Kotani A, Harada Y and Shin S 2002 *J. Phys. Soc. Japan* **71** 347
[31] Newman R and Chrenko R 1959 *Phys. Rev.* **114** 1507
[32] Figgis N B and Hitchman M A 2000 *Ligand Field Theory and its Applications* (New York: Wiley)
[33] Bersuker I B 1996 *Electronic Structure and Properties of Transition Metal Compounds* (New York: Wiley)
[34] Cowan R D 1981 *The Theory of Atomic Structure and Spectra* (Berkeley, CA: University of California Press)
[35] Slater J C 1960 *Quantum Theory of Atomic Structure* (New York: McGraw-Hill)
[36] Sugano S, Tanabe Y and Kamimura H 1970 *Multiplets in Transition-Metals Ions in Crystals* (New York: Academic)
[37] Butler P H 1981 *Point Group Symmetry Applications: Methods and Tables* (New York: Plenum)
[38] Thole B T, van der Laan G and Butler P H 1988 *Chem. Phys. Lett.* **149** 295
[39] Gorshülter A and Merz H 1994 *Phys. Rev.* B **49** 17293
[40] Fromme B, Schmitt M, Kisker E, Gorshülter A and Merz H 1994 *Phys. Rev.* B **50** 1874
[41] Fromme B 2001 *d–d Excitations in Transition-Metal Oxides* (Berlin: Springer)
[42] Fujimori A and Minami F 1984 *Phys. Rev.* B **30** 957
[43] de Groot F M F, Kuiper P and Sawatzky G A 1998 *Phys. Rev.* B **57** 14584
[44] de Groot F M F, Fuggle J C, Thole B T and Sawatzky G A 1990 *Phys. Rev.* B **42** 5459
[45] Gusmeroli R and Dallera C, unpublished
[46] Tanaka S, Kayanuma Y and Kotani A 1990 *J. Phys. Soc. Japan* **59** 1488
[47] Sugano S and Shulman R G 1963 *Phys. Rev.* **130** 517
[48] van der Laan G, Zaanen J, Sawatzky G A, Karnatak R and Esteva J-M 1986 *Phys. Rev.* B **33** 4253